

Approximating Accelerator Impedances with Resonator Networks

Brian J. Vaughn*

Fermi National Accelerator Laboratory, Batavia, Illinois 60510

It is common in the accelerator community to use the impedance of accelerator components to describe wake interactions in the frequency domain. However, it is often desirable to understand such wake interactions in the time domain in a general manner for excitations that are not necessarily Gaussian in nature. The conventional method for doing this involves taking the inverse Fourier Transform of the component impedance, obtaining the Green's Function, and then convolving it with the desired excitation distribution. This method can prove numerically cumbersome, for a convolution integral must be evaluated for each individual point in time when the wake function is desired. An alternative to this method would be to compute the wake function analytically, which would sidestep the need for repetitive integration. Only a handful of cases, however, are simple enough for this method to be tenable. One of these cases is the case where the component in question is an RLC resonator, which has a closed-form analytical wake function solution. This means that a component which can be represented in terms of resonators can leverage this solution. As it happens, common network synthesis techniques may be used to map arbitrary impedance profiles to RLC resonator networks in a manner the accelerator community has yet to take advantage of. In this work, we will use Foster Canonical Resonator Networks and partial derivative descent optimization to develop a technique for synthesizing resonator networks that well approximate the impedances of real-world accelerator components. We will link this synthesis to the closed-form resonator wake function solution, giving rise to a powerful workflow that may be used to streamline beam dynamics simulations.

1. Introduction

Wake field and impedance modeling of accelerator components is a critical aspect of the accelerator design process given the strong electromagnetic interactions between the particle beam and its surroundings. Because of the implications such interactions have on the beam's stability and dynamic evolution over time, much effort has been devoted to the electromagnetic simulation of accelerator components, resulting in the development and use of numerical codes such as CST Particle Studio [1], GdfidL, [2], Superfish [3], etc. While these codes are powerful in their ability to model E/M fields, they do not typically output the Green's Function of an accelerator component. That is, they do not give as an output the response of the component to a single moving point charge (impulse current), which would allow for the response of an arbitrary charge distribution to be found via convolution of the impulse current response with the greater distribution. Instead, the primary output is typically the wake function of a specified Gaussian excitation bunch distribution or the frequency-domain impedance of the component, which may be moved to the time-domain via an inverse Fourier transform and convolved with an arbitrary excitation bunch current to obtain a wake function [4]. Restricting ourselves to the longitudinal regime, we may represent this formalism in terms of a longitudinal wake voltage $V(t)$, a bunch excitation current $I(t)$, and an accelerator component impulse response (Green's Function) $z(t)$, all with respective Fourier Transforms $\tilde{V}(\omega)$, $\tilde{I}(\omega)$, and $\tilde{Z}(\omega)$. To simulate time-dependent beam dynamics, we are often interested in $V(t)$, which is the potential (work done per unit charge) experienced by a particle that enters the wake field of an accelerator component at time t excited by a bunch represented by $I(t)$. The relationships between these quantities are as follows:

$$V(t) = I(t) * z(t) = \int_{-\infty}^{\infty} I(t - \tau)z(\tau)d\tau, \quad (1a)$$

$$\tilde{V}(\omega) = \tilde{I}(\omega)\tilde{Z}(\omega). \quad (1b)$$

Again, if $\tilde{Z}(\omega)$ is the output of the simulation, the only way to obtain $z(t)$ is to conduct an inverse Fourier transform. Furthermore, even if $z(t)$ is on hand, the numerical computation of $V(t)$ requires the evaluation of a convolution integral (which must be truncated in the numerical context) for every time point of interest, which can be quite computationally expensive. These factors present a significant inconvenience for many accelerator modeling problems. One way around this obstacle would be to obtain an analytical result for $V(t)$, which would allow for $V(t)$ to be known at every time t without the need to conduct the convolution integral over and over, though an analytical result is difficult to achieve in general. There is, however, a case quite common in the accelerator space where an analytical result is available, namely, the case where the accelerator component in question is a parallel RLC resonator. Recently, in fact, a closed-form expression was derived for the wake potential $V(t)$ over a parallel RLC resonator excited by a bunch current $I(t)$ with Fourier Transform

*bvaughn@fnal.gov

$\tilde{I}(\omega)$. This expression is quoted below [5]:

$$V(t) = \frac{\omega_r R}{Q} \left(\frac{1}{r^+ - r^-} \right) (r^+ \tilde{I}(r^+) e^{jr^+ t} - r^- \tilde{I}(r^-) e^{jr^- t}), \quad (2)$$

$$r^\pm = \frac{\omega_r}{2} (j/Q \pm \sqrt{4 - \frac{1}{Q^2}}). \quad (3)$$

Where R is the resonator shunt resistance, ω_r is the resonant frequency, and Q is the quality factor. Note that this expression is truly closed-form, whereas, to the author's knowledge, expressions historically used to compute wake functions of parallel RLC resonators have involved the Error Function, which cannot be expressed with elementary functions [6]. Note that eqn. (2) is valid only if $\tilde{I}(\omega)$ has no poles (i.e., is holomorphic). If this is not the case, then eqn. (17a) of [5] is to be used instead, though that expression will not be quoted here due to its unnecessary complexity regarding the discussion herein. It should also be stated that eqns. (2) and (3) here are slightly different than the equations in [5] (eqns. (5b) and (13a) specifically). This is because the development in [5] invoked the change of variables $u \equiv \frac{\omega}{\omega_r}$ and then made evaluations in the u -domain. Here, the Fourier Transform evaluations are made in the ω -domain and the r^\pm definition includes ω_r as a result.

Due to the simplicity of the expression above, a reasonable strategy for wake potential modeling would be to approximate the impedance of the component in question using RLC resonators. This technique is not new and is a fairly common practice in the accelerator community [4], [7-9]. However, methods for executing this approximation appear to be primarily empirical in nature, and thus limited in the accuracy and sophistication of the resulting resonator networks. In other fields, however, optimization techniques along with utilization of a Foster Canonical Network (FCN) (more on this below) have been leveraged to represent generalized impedance responses in terms of RLC resonators [10]-[15]. Here, we will do the same, developing a partial-derivative-based procedural search algorithm that may be used to map broadband accelerator component data to quasi-equivalent resonator networks. The results of this effort, then, will provide a robust technique for mapping complex impedance responses to the time domain while bypassing the need for repetitive computations at different time points. The outline of the following sections is as follows: first, the FCN will be discussed in more detail. Next, the optimization algorithm used for this study will be described. Finally, examples will be given for the networks obtained when the optimization scheme is applied to the impedance data of actual accelerator components used in real machines today.

2. Foster Canonical Networks

In 1924, Ronald Foster proved an impactful network analysis theorem stating that general lossless impedance profiles or arbitrary networks may be described in terms of odd functions of frequency composed of alternating resonances and anti-resonances [10]. From there, it follows that one can synthesize non-unique approximate networks for arbitrary impedances that take one of the two forms shown below [10], [16]:

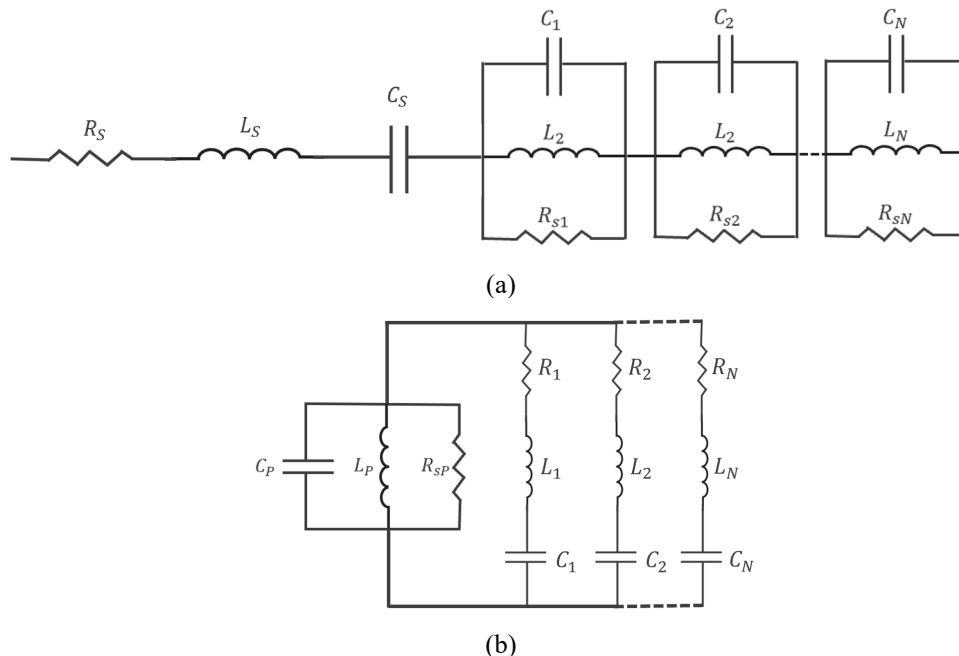


FIG. 1. Foster Canonical resonator networks used to synthesize impedance responses. The Form I variant (a) is made primarily of parallel RLC resonators in series with each other as well as one series RLC, whereas Form II (b) consists of series RLC's in parallel with each other as well as one parallel RLC.

As the figure above shows, the canonical forms either consist of series-connected parallel resonators with one series resonator or parallel-connected series resonators with one parallel resonator. Note that the circuits in the figure above contain resistive elements, which were not included in Foster's original formulation. Real passive networks, however, contain loss in general, so the canonical forms above were extended in an intuitive manner by adding resistors to the resonators, thus making their Q 's finite without violating Foster's Reactance Theorem. Both forms may be used for network synthesis, but Form I above is far more applicable to accelerator fields. This is because of the interaction between the impedances and the bunch excitation current $I(t)$. If the resonators are in series, then they each experience the same $I(t)$, which means that the total wake potential is merely the summation of the potentials developed over each individual resonator. For that reason, we will only consider Form I going forward.

One aspect of the above Form I circuit that must be developed further is the presence of the series RLC resonator. Since the development in [5] was geared toward RF cavities, only parallel RLC resonators were considered. The applicable theoretical treatment for the case of the series RLC resonator is, however, straightforward. This treatment is detailed thusly. Consider a series RLC resonator with an impedance described by the expression below:

$$Z_s(\omega) = R_s \left[1 - jQ_s \left(\frac{\omega_{rs}}{\omega} - \frac{\omega}{\omega_{rs}} \right) \right], \quad (4)$$

where R_s is the resonator series resistance, Q_s is the resonator quality factor, and ω_{rs} is the resonant frequency. Since we are interested in the convolution of the above expression's inverse Fourier Transform with the bunch current $\tilde{I}(\omega)$, we are equivalently interested in the inverse Fourier Transform of $\tilde{I}(\omega)Z_s(\omega)$. We may then represent the wake potential developed over the series RLC resonator as

$$V_s(t) = \check{F}^{-1} \left(R_s \tilde{I}(\omega) + \frac{R_s \omega_{rs} Q_s}{j\omega} \tilde{I}(\omega) + j\omega \frac{R_s Q_s}{\omega_{rs}} \tilde{I}(\omega) \right). \quad (5)$$

From well-documented Fourier Transform rules, we may evaluate this expression by inspection as

$$V_s(t) = R_s I(t) + R_s \omega_{rs} Q_s \int_{-\infty}^t I(t) dt + \frac{R_s Q_s}{\omega_{rs}} \frac{dI(t)}{dt}. \quad (6)$$

Invoking eqn. (2), we may now express the total wake potential developed over the Form I FCN:

$$V_{tot}(t) = R_s I(t) + R_s \omega_{rs} Q_s \int_{-\infty}^t I(t) dt + \frac{R_s Q_s}{\omega_{rs}} \frac{dI(t)}{dt} + \sum_1^N \frac{\omega_{rn} R_n}{Q_n} \left(\frac{1}{r_n^+ - r_n^-} \right) (r_n^+ \tilde{I}(r_n^+) e^{j\omega_{rn} r_n^+ t} - r_n^- \tilde{I}(r_n^-) e^{j\omega_{rn} r_n^- t}). \quad (7)$$

Note that the n subscripts denote that the parameter belongs to the n^{th} resonator in the parallel RLC chain. Note also that the number of parallel resonators N depends on the problem at hand. Typically, a larger N will result in a stronger approximation, but this increases the complexity of the optimization. This tradeoff will be discussed further below. We are now prepared to discuss the optimization process. While many optimization techniques are applicable to the current problem, the technique used here will rely on iterative and procedural partial derivative descent. This will be outlined in the following section.

3. Procedural Partial Derivative Descent

The optimization method herein uses the gradient descent technique as a basis, which minimizes a function by systematically adjusting its parameters in a direction dictated by the opposite value of the function's gradient [17]. That is, one may minimize a function $f(\mathbf{x})$ iteratively by choosing an initial guess \mathbf{x}_0 and executing the update algorithm:

$$\mathbf{x}_{p+1} = \mathbf{x}_p - \boldsymbol{\gamma} \cdot \nabla f(\mathbf{x}_p), \quad (8)$$

where $\boldsymbol{\gamma}$ is the step size vector and is chosen by the designer to facilitate the speed of convergence. Note that each element of $\boldsymbol{\gamma}$ is greater than 0. In conventional gradient descent, $\boldsymbol{\gamma}$ is instead a scalar with an optimal value determined via a line search at every step. The optimal value is determined by comparing the gradients at \mathbf{x}_p and \mathbf{x}_{p+1} and stopping the search when these two gradients are orthogonal [17]. If the gradient is not particularly well-behaved or if one does not wish to conduct a search at each iteration, static values or alternative adaptive strategies may be used. In either case, this value must be chosen with care. If the value is too big, the algorithm may enter an unstable trajectory and fail to converge properly. If the value is too small, convergence may take excessively long and convergence on local minima becomes more likely. We will discuss this step size further below. Our first step is to establish an appropriate $f(\mathbf{x})$ for the impedance approximation problem. Consider an impedance $Z_0(\omega)$ defined on the interval $\omega_1 \leq \omega \leq \omega_2$ that we wish to approximate with an

impedance $Z_F(\omega)$ described by a Form I FCN. We define a mean squared error parameter ε as follows:

$$\varepsilon = \frac{1}{\omega_2 - \omega_1} \int_{\omega_1}^{\omega_2} |Z_0(\omega) - Z_F(\omega)|^2 d\omega. \quad (9)$$

This is the function we wish to minimize over the prescribed frequency interval. Traditional gradient descent experiences difficulty minimizing this function, however, due to the poor conditionality of its gradient. To demonstrate this, we express the gradient of ε as follows:

$$\nabla \varepsilon = \frac{1}{\omega_2 - \omega_1} \int_{\omega_1}^{\omega_2} -2[\operatorname{Re}(Z_0(\omega)) - \operatorname{Re}(Z_F(\omega))] \nabla[\operatorname{Re}(Z_F(\omega))] - 2[\operatorname{Im}(Z_0(\omega)) - \operatorname{Im}(Z_F(\omega))] \nabla[\operatorname{Im}(Z_F(\omega))] d\omega. \quad (10)$$

Each parallel resonator has three free parameters; R_n , Q_n , and ω_{rn} , whereas the series resonator is described by R_s , Q_s , and ω_{rs} . We evaluate the gradients in the equation above by taking the partial derivatives of the superposed impedance expression with respect to each free variable. Recall that the impedance of the n^{th} parallel resonator in the network may be expressed as

$$Z(\omega) = \frac{R_n}{1 - jQ_n \left(\frac{\omega_{rn}}{\omega} - \frac{\omega}{\omega_{rn}} \right)}. \quad (11)$$

Using eqn. (4) and eqn. (11), we obtain the following partial derivatives:

$$\frac{\partial Z_F(\omega)}{\partial R_n} = \frac{1}{1 + Q_n^2 \left(\frac{\omega_{rn}}{\omega} - \frac{\omega}{\omega_{rn}} \right)^2} + j \frac{Q_n \left(\frac{\omega_{rn}}{\omega} - \frac{\omega}{\omega_{rn}} \right)}{1 + Q_n^2 \left(\frac{\omega_{rn}}{\omega} - \frac{\omega}{\omega_{rn}} \right)^2}, \quad (12a)$$

$$\frac{\partial Z_F(\omega)}{\partial Q_n} = \frac{-2R_n Q_n \left(\frac{\omega_{rn}}{\omega} - \frac{\omega}{\omega_{rn}} \right)^2}{\left[1 + Q_n^2 \left(\frac{\omega_{rn}}{\omega} - \frac{\omega}{\omega_{rn}} \right)^2 \right]^2} + j \frac{\left[\left(\frac{\omega_{rn}}{\omega} - \frac{\omega}{\omega_{rn}} \right) - Q_n^2 \left(\frac{\omega_{rn}}{\omega} - \frac{\omega}{\omega_{rn}} \right)^3 \right]}{\left[1 + Q_n^2 \left(\frac{\omega_{rn}}{\omega} - \frac{\omega}{\omega_{rn}} \right)^2 \right]^2}, \quad (12b)$$

$$\frac{\partial Z_F(\omega)}{\partial \omega_{rn}} = \frac{-2R_n Q_n^2 \left(\frac{1}{\omega} + \frac{\omega}{\omega_{rn}^2} \right) \left(\frac{\omega_{rn}}{\omega} - \frac{\omega}{\omega_{rn}} \right)}{\left[1 - Q_n^2 \left(\frac{\omega_{rn}}{\omega} - \frac{\omega}{\omega_{rn}} \right)^2 \right]^2 + 4Q_n^2 \left(\frac{\omega_{rn}}{\omega} - \frac{\omega}{\omega_{rn}} \right)^2} + j \frac{R_n Q_n \left(\frac{1}{\omega} + \frac{\omega}{\omega_{rn}^2} \right) \left[1 - Q_n^2 \left(\frac{\omega_{rn}}{\omega} - \frac{\omega}{\omega_{rn}} \right)^2 \right]}{\left[1 - Q_n^2 \left(\frac{\omega_{rn}}{\omega} - \frac{\omega}{\omega_{rn}} \right)^2 \right]^2 + 4Q_n^2 \left(\frac{\omega_{rn}}{\omega} - \frac{\omega}{\omega_{rn}} \right)^2}, \quad (12c)$$

$$\frac{\partial Z_F(\omega)}{\partial R_s} = 1 - jQ_s \left(\frac{\omega_{rs}}{\omega} - \frac{\omega}{\omega_{rs}} \right), \quad (12d)$$

$$\frac{\partial Z_F(\omega)}{\partial Q_s} = -jR_s \left(\frac{\omega_{rs}}{\omega} - \frac{\omega}{\omega_{rs}} \right), \quad (12e)$$

$$\frac{\partial Z_F(\omega)}{\partial \omega_{rs}} = -jR_s Q_s \left(\frac{1}{\omega} + \frac{\omega}{\omega_{rs}^2} \right). \quad (12f)$$

Note the above expressions are broken up into their real and imaginary parts since, in this case,

$$\nabla[\operatorname{Re}(Z_F(\omega))] = \operatorname{Re}(\nabla[Z_F(\omega)]), \quad (13a)$$

$$\nabla[\operatorname{Im}(Z_F(\omega))] = \operatorname{Im}(\nabla[Z_F(\omega)]). \quad (13b)$$

While not especially apparent by inspection, the partial derivatives with respect to the ω_r parameters in both the series and parallel cases are many orders of magnitude smaller than those with respect to the R and Q values. This is due to the $\left(\frac{1}{\omega} + \frac{\omega}{\omega_r^2} \right)$ terms present in the ω_r partial derivative expressions, which are far smaller than the $\left(\frac{\omega_{rn}}{\omega} - \frac{\omega}{\omega_{rn}} \right)$ terms in the other derivatives for high frequencies (note that accelerator impedances are routinely computed well into the GHz range). This means that the step size vector components that correspond to the ω_r parameters must be far larger than the other components, otherwise the resonant frequencies will barely change from update to update. This makes the step size vector problem-dependent in a manner that is challenging to generalize. To overcome this problem, we will modify the gradient descent technique by updating parameters individually instead of simultaneously. Further, we will apply a procedural component to the algorithm and limit which parameters can be modified under which circumstances. Specifically, the

parameters belonging to each individual resonator will be grouped together. The algorithm will only update the parameters of one resonator at a time, keeping the parameters of all other resonators static. Furthermore, the algorithm will prioritize updating the active resonator's resonant frequency first, only updating the resistance or Q parameters if changing the resonant frequency in any direction fails to reduce the value of ε . The direction in which the resonant frequency is updated is dependent on the corresponding partial derivative of ε . If the partial derivative is positive, the resonant frequency will be decreased by some static value chosen by the designer. If the derivative is negative, the resonant frequency will be increased.

When the error can no longer be decreased by modifying the resonant frequency of the active resonator, $\frac{\partial \varepsilon}{\partial R_n}$ is compared to $\frac{\partial \varepsilon}{\partial Q_n}$ ($\frac{\partial \varepsilon}{\partial R_s}$ and $\frac{\partial \varepsilon}{\partial Q_s}$ are compared if the active resonator is the series one). The parameter that corresponds to the larger partial derivative absolute value will be chosen to modify next. That is, if $\left| \frac{\partial \varepsilon}{\partial R_n} \right| > \left| \frac{\partial \varepsilon}{\partial Q_n} \right|$, then R_n will be updated as follows:

$$R_n^{update} = R_n - \gamma \frac{\partial \varepsilon}{\partial R_n}. \quad (14)$$

If the converse is true, then Q_n will be updated similarly:

$$Q_n^{update} = Q_n - \gamma \frac{\partial \varepsilon}{\partial Q_n}. \quad (15)$$

After the update is conducted, ε is computed again using the new values to determine if the error was reduced. If not, the update is undone and then recomputed using a smaller value of γ . In this way, we are able to utilize the advantages of both large and small step sizes. At the beginning of the loop, the step size is chosen to be large to facilitate faster convergence, but it is then decreased in magnitude to better approach the true minimum of ε . Note that for this algorithm, the step size is shared between R_n and Q_n , but this is not required in general. The comparison-update procedure is repeated until ε cannot be reduced without decreasing the step size beyond a certain user-defined threshold or if the change in ε between updates is smaller than some user-defined value. Once one of these conditions is met, the active resonator parameters are then saved and the algorithm moves to the next resonator to repeat the process. During the active resonator increment step, the algorithm also subtracts the impedance of the current resonator from target impedance (the target impedance is the impedance we are trying to develop a resonator network to approximate), minimizing the interference between the fits of the active and subsequent resonators. Once all the resonators have been updated, the code resets the target impedance to its initial value and rolls back to the first resonator to begin a new iteration of updates, once again moving from active resonator to active resonator while keeping the others static. The designer chooses how many of these update iterations occurs, but multiple iterations are necessary to ensure that ε cannot be reduced further with this technique since modifying each resonator changes the impedance landscape of the entire equivalent circuit. The designer also chooses the number of resonators to include in the network, with more typically being necessary to model more complex impedances. However, if the code determines that only a subset of the resonators is needed, it typically nulls the extraneous resonators by setting their R_n values to 0 (with the Q value being set to 0 as well if the active resonator is the series one). The code terminates when all iterations have been completed. The process outlined above is illustrated at a high level by the flowchart in Fig. 2. Note that the resonator parameters are initialized according to the designer. As with the step size, many initialization choices are possible, but setting Q_n equal to 1 and R_n equal to the maximum value of the real part of the current impedance tends to work well empirically. Setting both Q_n and R_n equal to 10 has also yielded acceptable results. The initial ω_{rn} values can either be the frequencies where the R_n maxima reside or they can be generated randomly relative to a uniform distribution depending on the problem at hand. The number of resonators to include is also up to the designer. Obviously, including more resonators will increase computation time, but this can result in a more sophisticated network frequency response if the target impedance profile has many features. Within reason, it is prudent to err on the side of more resonators instead of fewer, with the current study using 100 resonator networks as a base. It should be noted that the algorithm will not necessarily use all 100 resonators. When this happens, the algorithm, on its own, will only modify a subset of the resonators from iteration to iteration, nulling the impact of the extraneous resonators. Empirically, this is the typical result, meaning that adding more resonators gives rise to a point of diminishing returns for most problems. Where that point is exactly, however, is dependent on the problem itself and some experimentation may be needed. Nevertheless, 100 resonators as a general conservative starting point is empirically a tenable choice for consistent results. Furthermore, the time spent on extraneous resonators is comparatively minimal since a loop where no possible changes result in an ε reduction terminates much faster than a loop which moves the network many steps toward the ε minimization.

Before moving on, it should also be discussed whether the algorithm should be allowed to return negative values for R_n , Q_n , or ω_{rn} . While having such parameters in a real resonator would be nonphysical, this lack of physicality does not propagate to the approximated wake potential if the excitation current and target impedance profile are physical and all resonator parameters are real. There is quantitative basis for this claim. A nonphysical wake potential would be one with a nonzero imaginary part (negative wake potential values are allowed).

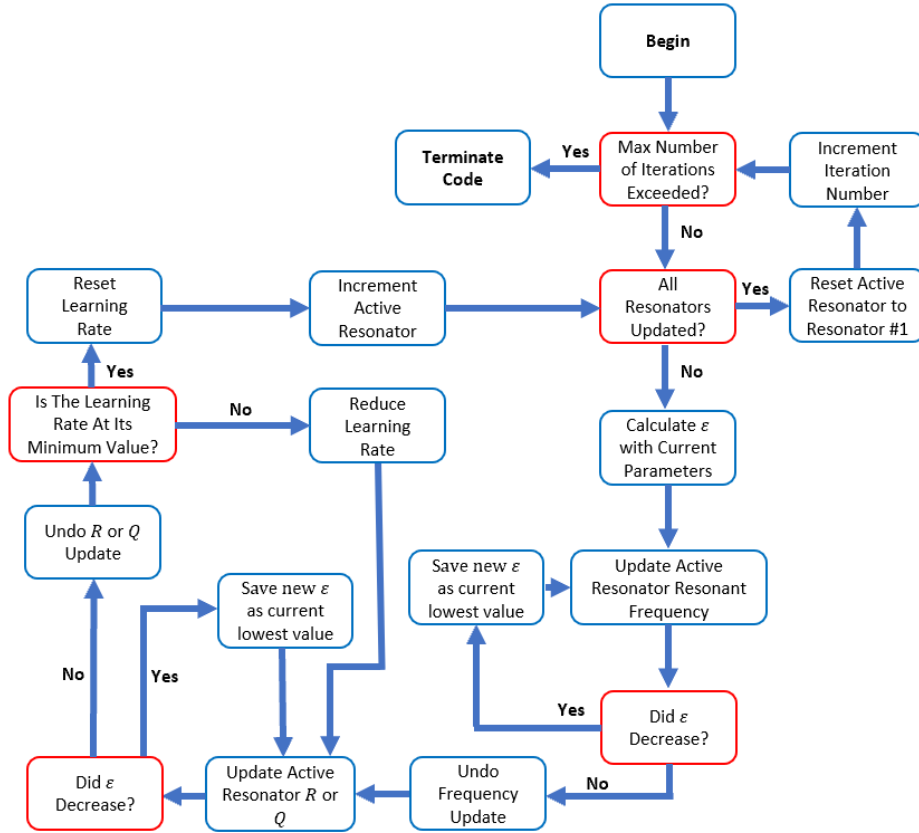


FIG. 2. High-level flowchart of partial derivative descent algorithm.

Recalling eqn. (7), we see that if the R values are real, there is no way for them to introduce an imaginary part regardless of their sign. The analysis of the effect of the Q and ω_r values, on the other hand, is less obvious, but still straightforward. The Q parameters appear both explicitly and within the r^\pm values along with the ω_r parameters. The explicit Q contributions, if real, do not cause issues for the same reasons the R contributions don't. To conclude that the r^\pm values also do not cause problems, we observe that r^+ and r^- have the same imaginary part and real parts of opposite sign. This means that $\tilde{I}(r_n^+)$ and $\tilde{I}(r_n^-)$ are complex conjugates of each other. To see why, we invoke the following Fourier Transform Property:

$$\tilde{F}(f(t)e^{j\omega_0 t}) = F(\omega - \omega_0). \quad (16)$$

This implies:

$$\tilde{F}\left(I(t)e^{j\left(\frac{-j\omega_r}{2Q}\right)t}\right)\Big|_{\omega=\pm\frac{\omega_r}{2}\sqrt{4-\frac{1}{Q^2}}} = \int_{-\infty}^{\infty} I(t)e^{j\left(\frac{-j\omega_r}{2Q}\right)t} e^{\pm j\frac{\omega_r}{2}\sqrt{4-\frac{1}{Q^2}}t} dt = \tilde{I}\left(\pm\frac{\omega_r}{2}\sqrt{4-\frac{1}{Q^2}} - \frac{j\omega_r}{2Q}\right) = \tilde{I}(r^\pm). \quad (17)$$

From Euler's Formula, we can expand the Fourier Integral:

$$\int_{-\infty}^{\infty} I(t)e^{j\left(\frac{-j\omega_r}{2Q}\right)t} e^{\pm j\frac{\omega_r}{2}\sqrt{4-\frac{1}{Q^2}}t} dt = \int_{-\infty}^{\infty} I(t)e^{\frac{\omega_r t}{2Q}} \cos\left(\frac{\omega_r}{2}\sqrt{4-\frac{1}{Q^2}}t\right) dt \pm j \int_{-\infty}^{\infty} I(t)e^{\frac{\omega_r t}{2Q}} \sin\left(\frac{\omega_r}{2}\sqrt{4-\frac{1}{Q^2}}t\right) dt. \quad (18)$$

Therefore, $\tilde{I}(r_n^+)$ and $\tilde{I}(r_n^-)$ are complex conjugates. By expanding terms, it is straightforward to see that $e^{j\omega_r r_n^+ t}$ and $e^{j\omega_r r_n^- t}$ are also complex conjugates, meaning $\tilde{I}(r_n^+)e^{j\omega_r r_n^+ t}$ and $\tilde{I}(r_n^-)e^{j\omega_r r_n^- t}$ are as well. Now, let

$$r^+ = -j\frac{\omega_r}{2}\left(-\frac{1}{Q} + j\sqrt{4-\frac{1}{Q^2}}\right) \equiv -jr_c, \quad (19a)$$

which means

$$r^- = -j \frac{\omega_r}{2} \left(-\frac{1}{Q} - j \sqrt{4 - \frac{1}{Q^2}} \right) \equiv -j\bar{r}_c. \quad (19b)$$

We now have

$$r^+ \tilde{I}(r^+) e^{jr^+t} - r^- \tilde{I}(r^-) e^{jr^-t} = -j(r_c \tilde{I}(r^+) e^{jr^+t} - \bar{r}_c \tilde{I}(r^-) e^{jr^-t}). \quad (20)$$

The terms in the parentheses represent the subtraction of some quantity from its complex conjugate, which results in a purely imaginary value. Since this is then multiplied by $-j$, we see that the expression in eqn. (20) is purely real regardless of the sign of Q or ω_r , provided they are both real. Finally, we note that since r^+ and r^- have the same imaginary part, $r^+ - r^-$ is purely real as well. Therefore, the wake potential given by eqn. (7) remains real even if the Q or ω_r of any of the resonators takes a negative value. In the next section, the results of applying the above algorithm to several accelerator impedance studies will be shown.

4. Results

To evaluate the efficacy of the presented technique, we will now map FCN's to three real-life accelerator impedance profiles across various frequency ranges using an implementation of the previously described algorithm in MATLAB. The first profile we will evaluate is the longitudinal impedance of the Lamberston magnets currently being used in the Fermilab Main Injector Ring [18]. The impedance given in [18] is shown in Fig. 3 along with the impedance of the mapped FCN synthesized by the algorithm presented above. Additionally, the resonator parameter outputs for this are given in Appendix I, as well as the code runtime to generate the network. The initial resonant frequencies for this example were generated based on real part impedance maxima as discussed in the previous section.

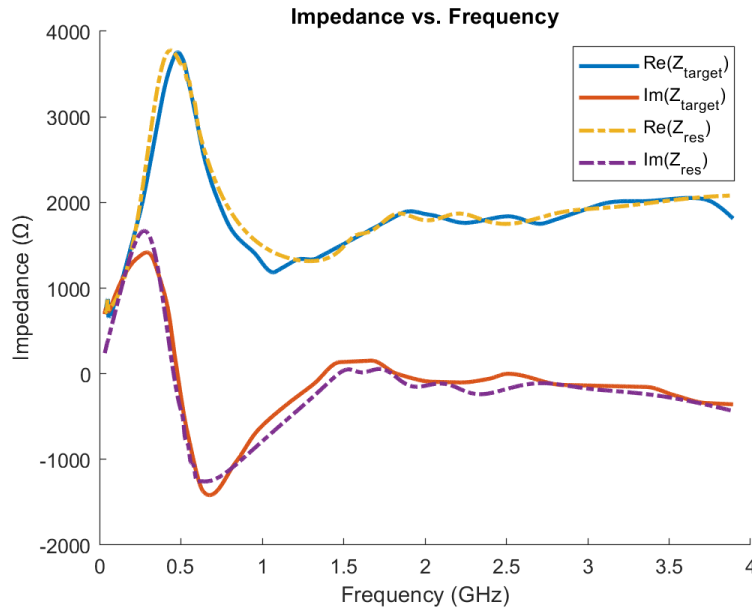


FIG. 3. Fermilab Main Injector Lamberston magnet and approximate resonator network impedances. The solid lines are the target impedance values and the dotted lines represent the impedance of the synthesized resonator network.

Fig. 3 shows very good agreement between the synthesized network impedance and the true values, indicating, at a minimum, that the technique presented here is appropriate for smooth broadband impedance profiles with few stark features. This network consists of 1 series resonator and 16 parallel resonators with various parameters and was generated over 5 iterations.

Next, we will consider the total broadband longitudinal impedance of the NCLS-II Storage Ring for a .3 mm bunch length, which is given in [19]. This impedance is given over a frequency span of 300 GHz and requires 30 parallel resonators to model. As with Fig. 3, the comparison between the target and synthesized network impedances for this case are given in Fig. 4. As with the Lamberston magnet example, the initial resonant frequencies used the locations of the real part impedance maxima as a starting point.

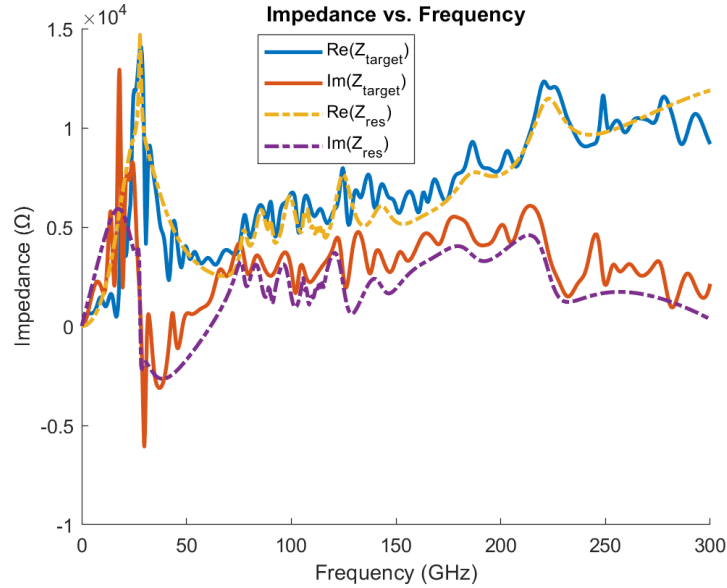


FIG. 4. NCLS-II Storage Ring and approximate resonator network impedances. The solid lines are the target impedance values and the dotted lines represent the impedance of the synthesized resonator network.

Here, the agreement between the synthesized and target impedance profiles is lower than with the Lamberston magnet case, which is expected since the frequency range is much wider with far more features. For instance, there is a spike in the imaginary part of the target impedance at around 20 GHz that is not captured by the resonator network. Additionally, there is a dip in the real part of the target impedance around 30 GHz that is also not captured. Nevertheless, the resonator network impedance follows the target impedance quite strongly overall, certainly well enough for first-order simulation studies.

Finally, we will consider the longitudinal impedance of a stripline kicker with two 90° electrodes, the impedance of which is given in [19] and [20]. As before, we compare this impedance to a synthesized resonator network impedance in Fig. 5. With this example, the initial resonant frequencies were generated randomly, as this yielded better results.

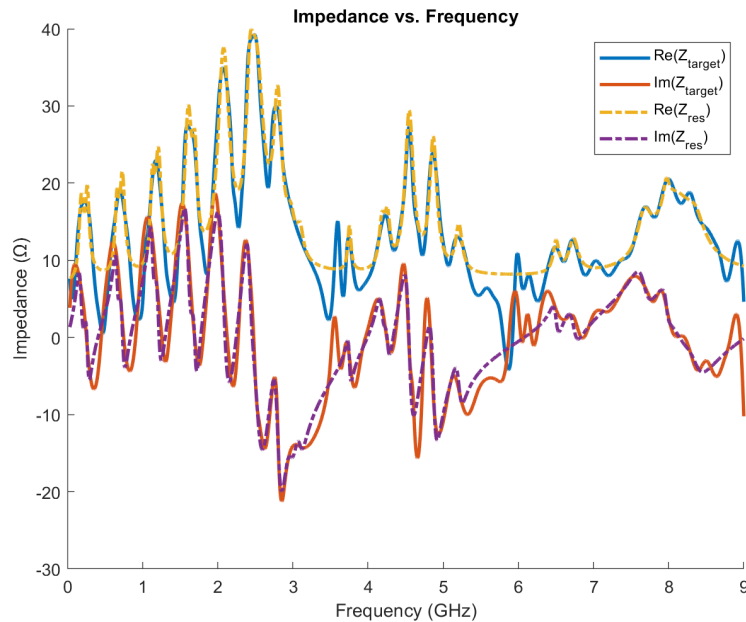


FIG. 5. Stripline kicker and approximate resonator network impedances. The solid lines are the target impedance values and the dotted lines represent the impedance of the synthesized resonator network.

Here, once more, we see good agreement between the synthesized network impedance and the target, though some of the oscillatory features in the real part of the impedance are not fully captured before 3 GHz. Nevertheless, the resonator network result outperforms the theoretical approximation of the kicker impedance at frequencies below 3 GHz, which is shown alongside the numerically calculated impedance in Fig. 6 of [19]. This indicates that the synthesized network impedance is an appropriate approximation since it matches the broadband target impedance well and constitutes an overall improvement over a theoretical approximation within the frequency range where the theoretical treatment is valid. Note that the algorithm for this network, as opposed to the previous examples, used all 100 resonators to properly capture the

asymmetric oscillations and other features. It should also be noted that several values of R_n and Q_n for this network are negative. This is acceptable given the discussion in the previous section.

5. Conclusion

In this work, we have developed a method to represent general real-life accelerator component impedance profiles in terms of synthesized RLC resonator networks using partial derivative descent optimization. We have applied this technique to three broadband frequency responses relevant to the accelerator field and have shown solid agreement between these profiles and the impedances of the synthesized networks. This technique is highly useful since the wake potentials of such resonator networks may be computed analytically in a straightforward manner, meaning that, once the network is generated, the components' wake potentials may be known at all time points without the need for repetitive convolution, saving significant time and computing resources during beamline simulations. As such, the work presented here can be used to great effect during accelerator design efforts.

References

- [1] CST Particle Studio, <https://www.3ds.com/products/simulia/electromagnetic-simulation/particle-dynamics>.
- [2] W. Bruns, <http://www.gdfidl.de>.
- [3] SuperFish, <https://laacg.lanl.gov/laacg/services/>.
- [4] M. Migliorati and L. Palumbo, "Multibunch and Multiparticle Simulation Code with an Alternative Approach to Wakefield Effects," in *Physical Review Special Topics-Accelerators and Beams*, **18**, 031001 (2015).
- [5] B. J. Vaughn, "A Simple, Flexible Technique for RF Cavity Wake-Field Calculations," in *Journal of Instrumentation*, **18**, P11004 (2023).
- [6] Chao et al., *Handbook of Accelerator Physics and Engineering*, World Scientific Publishing, Hackensack, NJ (2023).
- [7] E. Benedetto et. al., "Simulation study of electron cloud induced instabilities and emittance growth for the CERN Large Hadron Collider proton beam," in in *Physical Review Special Topics-Accelerators and Beams*, **8**, 124402 (2005).
- [8] E. Métral, "Fast High-Intensity Single-Bunch Transverse Coherent Instability in Synchrotrons due to a Broad-Band Resonator Impedance", CERN/PS 2001-035 (AE), July 2001.
- [9] V. Smaluk, "Beam-Based Impedance Measurement Techniques," in *Proceedings of 58th ICFA Advanced Beam Dynamics Workshop on High Luminosity Circular e+e- Colliders, Daresbury, UK, October, 2016*.
- [10] R. M. Foster, "A Reactance Theorem," in *The Bell System Technical Journal*, **3** (2), pp. 259-267, (1924).
- [11] Y. Wang and J. Z. Li, "An Equivalent Circuit Modeling Method for Ultra-Wideband Antennas," in *Progress In Electromagnetic Research*, **82**, pp. 433-445, (2008).
- [12] D. Dončov et. al., "Extended Foster Approach for Equivalent Circuit Synthesis of Lossy Microwave Circuits," in *Proceedings of 19th Telecommunications Forum, Belgrade, Serbia, November, 2011*.
- [13] E. Fatima et. al., "Circuit Modelling of Broadband Antenna Using Vector Fitting and Foster Form Approaches for IoT Applications," in *Electronics*, **11** (22), 3724, (2022).
- [14] S. B. T. Wang et. al., "Circuit Modeling Methodology for UWB Omnidirectional Small Antennas," in *IEEE Journal on Selected Areas in Communications*, **24** (4), pp. 871-877, (2006).
- [15] K. Sayidmarie and L. Yahya, "Modeling of Dual-Band Crescent-Shape Monopole Antenna for WLAN Applications," in *International Journal of Electromagnetics and Applications*, **4** (2), pp. 31-39, (2014).
- [16] S. Ramo et al., *Fields and Waves in Communication Electronics*, John Wiley & Sons, Inc., Hoboken, NJ (1994).
- [17] E. K. P. Chong and S. H. Žak, *An Introduction to Optimization*, John Wiley & Sons, Inc., Hoboken, NJ (2013).
- [18] "The Fermilab Main Injector Technical Design Handbook," United States, 1994, <https://doi.org/10.2172/1127909>.
- [19] A. Blednykh et. al., "Impedance Modeling and its Application to the Analysis of the Collective Effects," in *Physical Review Accelerators and Beams*, **24**, 104801, (2021).
- [20] A. Blednykh et. al., "Beam Impedance and Heating Analysis of the Diagnostic Stripline," in *Nucl. Instrum. Methods Phys. Res., Sect. A*, **963**, 163729, (2020).

Appendix I

Below are tables listing the resonator parameters of the networks synthesized in the three examples of Section 4. Note that, if a table contains fewer than 100 resonators, then the algorithm returned null values for the resonators not included, indicating their lack of necessity. Note also that Resonator #1 for all the networks is the series RLC. Each table caption also contains the algorithm runtime for each example on a generic laptop with 32 GB of RAM as well as the number of iterations completed.

Resonator Number	R (Ω)	Q	f _r (GHz)
1	695.6189271	0	4
2	3061.165433	1	0.436
3	1311.930262	1	4.082
4	390.5001476	4.712186274	2.21
5	181.4306801	3.965788261	2.842
6	536.217187	4.543105508	1.826
7	160.2546347	24.77271266	0.586
8	163.11532	24.29191781	0.552
9	126.5849183	1316.866073	0.05
10	125.7083409	1320.051448	0.049

11	122.2372349	1274.958927	0.051
12	120.6887107	1237.364837	0.048
13	112.1013301	1234.916788	0.047
14	112.4928412	1198.894385	0.052
15	168.5624404	24.50549518	0.519
16	215.8332079	7.451141111	1.568
17	94.50700975	1063.261728	0.053

Table A.1. Resonator parameters for the network synthesized to approximate the Fermilab Main Injector Lamberston magnet longitudinal impedance. 5 iterations. Runtime = 3 min.

Resonator Number	R (Ω)	Q	f _r (GHz)
1	0	0	300
2	5198.1451	21.2441703	27.832
3	12337.9601	1	339.61
4	9452.64631	1	26.787
5	4666.20179	11	124.65
6	4025.13104	11	99.261
7	3382.48986	11	85.623
8	2094.21066	10.9884028	142.84
9	1919.37856	46.7412581	107.8
10	2139.06261	18.0826521	77.345
11	2335.23576	13.5567097	222.48
12	1572.74661	7.43761208	221.41
13	1207.84189	9.45003197	186.03
14	834.751323	148.202949	89.991
15	983.598468	50.4323558	110.17
16	598.720206	120.517882	91.088
17	912.363757	66.6852037	112.28
18	862.039661	5.3971679	185.16
19	1202.52388	80.6345988	106.09
20	755.805952	92.5530311	115.05
21	480.60856	234.720583	90.624
22	888.477338	5.01303663	163.09
23	522.098108	166.148267	89.357
24	661.998875	123.95807	113.96
25	298.293384	541	90.352
26	419.748066	187.417967	113.25
27	90.9196336	691	90.472
28	80.1254642	721	90.234
29	0.01711689	691	90.235
30	0.00233523	691	90.235
31	10.0003186	691	90.474

Table A.2. Resonator parameters for the network synthesized to approximate the NSLS-II total longitudinal impedance. 5 iterations. Runtime = 70 min.

Resonator Number	R (Ω)	Q	f _r (GHz)
1	12.19772911	1.11323568	0.225021523
2	19.22202327	2.934148588	0.698074272
3	13.92773618	3.656775963	1.176127579
4	23.63309888	3.849721156	1.596174417
5	29.06199253	7.549918617	2.074227724
6	37.34173614	10.54813445	2.487273782
7	12.81716377	3.849702736	2.774305788
8	15.08488578	30.07010268	3.596397457
9	12.98892641	19.57860456	3.742413739
10	15.92137084	17.82554248	4.230468161
11	27.33505342	34.20398723	4.546503401
12	23.99433913	31.03817102	4.863538753
13	-18.40020959	2.351887848	5.191575332

14	0.585368187	-2.916066794	5.579618602
15	10.935892	24.79179408	5.987664102
16	8.157196511	29.47475557	6.139681053
17	11.76482029	2.255767743	6.492720419
18	-67.33059102	0.1453626	6.718745623
19	-0.22842353	-7.221489971	7.030780417
20	-12.62646613	5.999752737	7.693854355
21	17.29887078	17.08971109	7.996888145
22	14.87008351	13.68732476	8.277919483
23	10	10	8.149905208
24	0.936950854	10	7.891876436
25	10	10	8.998999888
26	0.379444693	10	7.78286428
27	10	10	0.362036802
28	-6.548679649	10	4.916544664
29	10	10	8.978997658
30	3.910847888	10	4.614510985
31	1.64220667	10	7.865873536
32	10	10	0.661070146
33	10	0.361000484	8.888987621
34	-4.16752294	10	8.306922717
35	8.184893978	10	5.092564291
36	7.972849473	10	3.901431471
37	6.070945386	10	3.061337794
38	10	10	6.495720754
39	10	10	0.154013605
40	4.892000011	10	3.386374038
41	10	10	8.306922717
42	-0.572404028	10	4.932546448
43	0.401245548	10	4.281473849
44	-3.282140008	10	4.484496487
45	10	10	2.80230891
46	10	0.330756392	8.559950931
47	10	0.359070334	8.838982045
48	2.38235016	10	4.63751355
49	-15.46477073	10	8.93399264
50	6.064634346	10	4.120455894
51	-4.912296784	10	3.852426006
52	-16.87721086	5.618030212	1.944213226
53	10	10	1.765193264
54	10	0.141239052	7.500832831
55	10	3.674841674	6.548726664
56	-1.36938276	10	4.78252972
57	10	0.130577679	7.467829151
58	8.919671577	10	4.622511877
59	4.523544116	10	4.981551913
60	10	10	1.944213226
61	10	10	5.303587822
62	5.853504257	10	1.312142746
63	2.604038227	10	0.500052191
64	10	10	6.159683283
65	9.107723561	10	5.489608565
66	10	10	2.001219583
67	-7.642896794	10	3.675406267
68	10	10	5.681629977
69	10	10	5.011555258

70	10	10	1.176127579
71	10	10	1.549169176
72	10	10	0.040000892
73	4.885590023	10	3.7824182
74	2.838449172	10	4.412488458
75	-8.904057209	10	1.465159808
76	-44.90503725	1.359428645	6.01266689
77	10	10	0.192017843
78	10	10	1.105119661
79	10	0.079877003	8.570952158
80	10	0.361213449	8.783975912
81	10	10	0.309030891
82	4.469725594	10	4.461493922
83	2.857975316	10	7.768862719
84	10	10	2.210242891
85	10	0.192921078	7.513834281
86	10	4.2694811	7.32881365
87	10	10	5.672628973
88	10	10	0.05200223
89	-12.25198492	10	3.437379726
90	-28.69527147	9.918168535	8.142904427
91	-21.3520451	10	6.133680384
92	8.291922759	10	3.429378834
93	-8.120286858	10	5.699631984
94	-3.707707069	10	2.213243225
95	8.967940828	10	5.156571429
96	10	0.365411268	8.836981822
97	8.518395337	10	7.651849671
98	-2.322655242	10	2.573283372
99	8.831817142	10	6.152682503
100	4.127278056	10	3.243358091

Table A.3. Resonator parameters for the network synthesized to approximate the stripline kicker total longitudinal impedance. 5 iterations. Runtime = 53 min.